

Heat, molecular vibrations, and adiabatic driving in non-equilibrium transport through interacting quantum dots

F. Haupt^{1,2}, M. Leijnse^{3,4}, H. L. Calvo^{1,2,5}, L. Classen^{1,2}, J. Splettstoesser^{1,2}, M. R. Wegewijs^{*,1,2,5}

¹ Institute for Theory of Statistical Physics, RWTH Aachen, 52056 Aachen, Germany

² JARA- Fundamentals of Future Information Technology

³ Center for Quantum Devices, Niels Bohr Institute, University of Copenhagen, DK-2100 Copenhagen, Denmark

⁴ Solid State Physics and Nanometer Structure Consortium (nmC@LU), Lund University, 221 00 Lund, Sweden

⁵ Peter Grünberg Institut, Forschungszentrum Jülich, 52428 Jülich, Germany

Received XXXX, revised XXXX, accepted XXXX

Published online XXXX

Key words: Molecular quantum dots, heat transport, time-dependent driving, thermoelectric effect.

* Corresponding author: e-mail m.r.wegewijs@fz-juelich.de

In this article we review aspects of charge and heat transport in interacting quantum dots and molecular junctions under stationary and time-dependent non-equilibrium conditions due to finite electrical and thermal bias. In particular, we discuss how a discrete level spectrum can be beneficial for thermoelectric applications, and investigate the detrimental effects of molecular vibrations on the efficiency of a molecular quantum dot as an energy converter.

In addition, we consider the effects of a slow time-dependent modulation of applied voltages on the transport properties of a quantum dot and show how this can be used as a spectroscopic tool complementary to standard dc-measurements. Finally, we combine time-dependent driving with thermoelectrics in a double-quantum dot system – a nanoscale analogue of a cyclic heat engine – and discuss its operation and the main limitations to its performance.

Copyright line will be provided by the publisher

1 Introduction Quantum dots are small man-made structures, with a length scale typically ranging from nanometres to a few microns. They can be realized in semiconductor heterostructures [1,2], semiconductor nanowires [3,4,5], nanotubes [6,7], graphene [8], or even with single molecules [9,10,11]. The name refers to the zero-dimensional nature of this class of systems, meaning that the wave function of charge carriers residing on the dot is confined in all spatial directions [12]. In a transport setup, a quantum dot is tunnel coupled to source and drain electrodes and a dc-current is established by applying a finite source-drain bias voltage. Because of the strong Coulomb repulsion between electrons localized on the dot and the relatively weak coupling to the electrodes, charge carriers are transferred through the device one-by-one, and transport can even be completely blocked at low voltages.

This phenomenon is known as Coulomb blockade [13]. In addition to the source and drain, there is often a gate electrode, which is only capacitively coupled to the quantum dot and can be used to electrostatically control the number of electrons on the dot, as well as the energy cost of adding more electrons, and thereby the conductance of the junction. In such a transistor geometry, the electronic current provides direct information on the quantum level-structure and classical charging energies of the dot itself. This generic description provides a good starting point even for systems as small as a single molecule or atom in a junction.

Applications of quantum dots as ultra-sensitive detectors [14], thermometers [15] or basic building blocks in quantum computers [16] have already been considered for a long time. Lately, the possibility of exploiting their prop-

Copyright line will be provided by the publisher

erties for energy conversion or cooling applications have also started to attract considerable attention. As an example, a refrigeration scheme based on resonant tunneling through quantum dots [17] has been recently demonstrated experimentally [18]. Theoretically, it has been shown that if a quantum dot is weakly tunnel coupled to a hot and a cold electrode, it can act as an efficient thermoelectric energy converter [19,20].

In conductors, heat is carried dominantly by electrons and the phononic contribution to the heat flow can be often neglected in first approximation. However, phononic heat currents set an ultimate limit to the properties of thermoelectric devices. Minimizing them is crucial to achieve efficient energy conversion and for cooling applications. In molecular quantum dots, phonons (quantized molecular vibrations), strongly affect not only the thermoelectric but also the transport properties of the device. In fact, an electric current can excite vibrations and even drive them out of equilibrium. This in turn affects the conductance of the junction, as well as its stability. For electronic applications, it can therefore be desirable to design (molecular) quantum dots with good thermal contacts to the electrodes, or other heat reservoirs.

The study of heat currents is relevant also in the case of time-dependently driven systems, as it carries information on the dissipation associated with the driving [21]. Time-dependently driven quantum dots have attracted a lot of attention in recent years, for the possibility of realizing quantized charge pumping [22,23,24] and reliable single-electron sources [25]. These have a realm of applications, ranging from metrology [26], to solid-state based quantum information. Spin-pumping has also been demonstrated [27]. Without thermal driving, time-dependent driving can be employed as a spectroscopic tool to investigate the dot. In fact, it has been shown that the charge pumped through the system in response to the ac-driving is sensitive to the microscopic detail of the potential landscape of the dot [23] and, in appropriate modulation setups, it provides information on the coupling asymmetry [28], or even on subtle renormalization effects due to tunneling [29]. Furthermore, an ac-driven quantum-dot system can also be operated as a nanoscale *cyclic* engine, exchanging heat and work with reservoirs with different temperatures or chemical potentials.

In this review, we discuss recent progress in the theoretical understanding of several aspects of charge and heat flow in quantum dot systems, both with non-equilibrium conditions induced by a stationary voltage or temperature gradient and by time-dependent driving of externally applied fields. The paper is organized as follows.

Section 2 summarizes the master equation approach employed for calculating the charge, the heat and the spin current through a quantum-dot device, based on lowest order tunneling processes and an expansion in the driving frequency.

Section 3 focuses on the thermoelectric effect. The physical origin of the thermoelectric effect is explained and the desirable electronic properties of a good thermoelectric material are discussed, along with the problems involved in finding real systems exhibiting these properties. In addition, the different contributions to the phononic heat current are discussed in some detail. All these aspects are then brought together in a simple model of a molecular thermoelectric device, where the sharp molecular orbitals provide a large thermoelectric effect, while electron-phonon coupling on the molecule, as well as coupling between quantized molecular vibrations and substrate phonon modes in the electrodes, give rise to significant losses.

Section 4 discusses time-dependent electronic transport and reviews recent progress on pumping in strongly interacting dots. Focusing on the slow driving regime, we exploit the geometric nature of the pumped currents and write them as the flux generated by a pseudo-magnetic field. As an application example, we consider a single-level quantum dot driven by time-dependent gate and bias voltages, where additional non-equilibrium effects are induced by a finite static bias. We use the pseudo-magnetic field to describe interaction-induced pumping and to investigate internal properties of the dot such as spin degeneracy and junction asymmetry in different regimes of the voltage bias.

Finally, as a further application example, section 5 investigates the heat current in the presence of time-dependent driving. For the case of a driven double-dot, we show that there are regimes where not only the charge current but also the heat current is quantized, and that in these regimes the double dot can be regarded as a nanoscale analog of the Carnot engine.

2 Microscopic model and transport theory The (molecular) quantum dot setup that we want to describe can be represented in general as a central device region that is tunnel coupled to electronic or bosonic reservoirs, which can usually be considered non-interacting. The corresponding Hamiltonian can be written as $H = H_D + H_{\text{res}} + H_{\text{coupl}}$, where H_D is the Hamiltonian of the device and is typically governed by many-body interactions. Without loss of generality, we can write $H_D = \sum_{\xi} E_{\xi} |\xi\rangle \langle \xi|$, where $|\xi\rangle$ denote the many-body eigenstates of the device, with energy E_{ξ} . The reservoirs are described by a quadratic (non-interacting) Hamiltonian H_{res} and we assume them to be held at separate equilibria with temperatures T_r (and chemical potentials μ_r , for the fermionic reservoirs). The coupling term H_{coupl} is bi-linear in the operators of the device and the reservoirs. The coupling to the reservoirs is quantitatively characterized by the coupling strength $\Gamma_r = 2\pi\nu_r |t_r|^2$, where t_r is the single-particle tunneling matrix element between the device and reservoir r , and ν_r is the density of states of the latter ($\hbar = k_B = e = 1$). Both t_r and ν_r are often assumed to be energy independent (wide-band limit).

In general, the Hamiltonian of the system H can depend on time due to some external time-dependent driving, i.e. $H(t) = H(\mathbf{u}(t))$, where $\mathbf{u}(t) \equiv \{u_i(t)\}$ are the driving parameters.

2.1 Master equation approach The explicit results presented in the following sections are based on a master equation approach (unless mentioned otherwise), where the state of the device is described in terms of the occupation probabilities $P_\xi(t)$ of its eigenstates. To lowest order in the tunneling, their evolution is governed by the Markovian master equation

$$\frac{d}{dt} \mathbf{P}(t) = \mathbf{W}_t \mathbf{P}(t), \quad (1)$$

with $\mathbf{P}(t) = \{P_\xi(t)\}$. The kernel \mathbf{W}_t can be written as a sum of independent contributions from the reservoirs $\mathbf{W}_t = \sum_r \mathbf{W}_{r,t}$, where the matrix element $[\mathbf{W}_{r,t}]_{\xi\xi'} \propto \Gamma_r$ represents the probability per unit time that a tunneling event from/to reservoir r induces the transition $|\xi'\rangle \rightarrow |\xi\rangle$, as given by Fermi's golden rule. The subscript t indicates that these rates have to be evaluated with the parameters of the Hamiltonian “frozen” at time t .

If the Hamiltonian H is time independent, the evolution kernel is also time independent $\mathbf{W}_t \rightarrow \mathbf{W}$, and in the long-time limit the system reaches the stationary state $\mathbf{P}^{(0)}$, which satisfies $\mathbf{W}\mathbf{P}^{(0)} = 0$.

Describing the dynamics of a driven systems in terms of Eq.(1), we implicitly assumed the time scale of the driving to be much slower than the electron life-time in the system. In this case, Eq. (1) can be solved by means of an adiabatic expansion for the occupation probabilities $\mathbf{P}(t) \rightarrow \sum_{k \geq 0} \mathbf{P}_t^{(k)}$, where $\mathbf{P}_t^{(k)} \propto (\Omega/\Gamma)^k$ in the case of harmonic driving [29]. Here, Ω is the driving frequency and Γ the characteristic tunnel rate of the system. The adiabatic expansion gives rise to the hierarchy of equations [29, 30]

$$\text{a) } \mathbf{W}_t \mathbf{P}_t^{(0)} = 0, \quad \text{b) } \mathbf{W}_t \mathbf{P}_t^{(k)} = \frac{d}{dt} \mathbf{P}_t^{(k-1)}. \quad (2)$$

Here, $\mathbf{P}_t^{(0)}$ is the solution of the problem with all parameters frozen at time t . It represents the steady state the system would relax into if it could instantaneously follow the modulation of the time-dependent parameters. We will therefore refer to it as the *instantaneous* solution. Corrections due to retardation effects are encoded in $\mathbf{P}_t^{(k>0)}$ and are governed by a competition of the time scales of the driving and of the response time contained in \mathbf{W}_t . The normalization conditions are $\text{Tr}\{\mathbf{P}_t^{(0)}\} = 1$, and $\text{Tr}\{\mathbf{P}_t^{(k>0)}\} = 0$, where the trace of a vector is defined as the sum of its components.

The above master equation approach can be rigorously derived [29, 30] starting from a real-time diagrammatic expansion of the reduced density matrix of the system [31, 32], and it is valid in the regime of weak coupling to the leads $\Gamma \ll T = \min\{T_r\}$ and slow driving $\Omega \ll \Gamma$.

2.2 Charge, spin and heat currents We are interested in the charge, heat and spin currents flowing in response to a time-dependent modulation of the parameters of the Hamiltonian and/or to an external bias voltage or temperature gradient. The electric current flowing out of lead $r = L, R$ is found from the derivative of the electron number $I_r(t) = \frac{d}{dt} \langle N_r \rangle$, where $N_r = \sum_{k\sigma} c_{rk\sigma}^\dagger c_{rk\sigma}$ is the occupation number operator in lead $r = L, R$. Similarly, the heat and spin currents are defined as $Q_r(t) = -\frac{d}{dt} \langle H_r - \mu_r N_r \rangle$ and $J_r(t) = -\frac{d}{dt} \langle S_r^z \rangle$, respectively, where $H_r = \sum_{k\sigma} \epsilon_{rk\sigma} c_{rk\sigma}^\dagger c_{rk\sigma}$ is the Hamiltonian of the lead and $S_r^z = \sum_{k\sigma} \frac{\sigma}{2} c_{rk\sigma}^\dagger c_{rk\sigma}$ is the projection of the lead spin on the quantization axis (chosen along the magnetic field if there is one) and $\sigma = \pm$ stands for spin \uparrow, \downarrow . A phononic heat current is defined in the same way, but with $\mu_r = 0$ and $H_r = \sum_{qr} \omega_{qr} b_{qr}^\dagger b_{qr}$.

The currents can be evaluated directly from the knowledge of the occupation probability $\mathbf{P}(t)$, being $R(t) = \text{Tr}\{\mathbf{W}_t^R \mathbf{P}(t)\}$, where $R \in \{I_r, Q_r, J_r\}$ and the kernels \mathbf{W}_t^R take into account the charge, the heat and the spin flowing from lead r into the device, respectively. For weak coupling to the leads ($\Gamma \ll T$), these kernels read as

$$\begin{aligned} [\mathbf{W}_t^{I_r}]_{\xi\xi'} &= -e(n_\xi - n_{\xi'}) [\mathbf{W}_{r,t}]_{\xi\xi'}, \\ [\mathbf{W}_t^{Q_r}]_{\xi\xi'} &= \{E_\xi - E_{\xi'} - \mu_r(n_\xi - n_{\xi'})\} [\mathbf{W}_{r,t}]_{\xi\xi'}, \\ [\mathbf{W}_t^{J_r}]_{\xi\xi'} &= (s_\xi - s_{\xi'}) [\mathbf{W}_{r,t}]_{\xi\xi'}. \end{aligned} \quad (3)$$

Here, E_ξ , n_ξ and s_ξ are the energy, the number of electrons and the spin in the device in the state $|\xi\rangle$, respectively.

In the case of slow harmonic driving, the expansion in the driving frequency carried out for $\mathbf{P}(t)$ results in an analogous expansion for the current $R(t) = \sum_{k \geq 0} R_t^{(k)}$, where $R_t^{(k)} = \text{Tr}\{\mathbf{W}_t^R \mathbf{P}_t^{(k)}\}$ is the contribution of order Ω^k to the current. The instantaneous contribution $R_t^{(0)}$ is the only non vanishing term in the stationary situation, and it is non-zero only if the system is brought out of equilibrium by means of a bias voltage or a temperature gradient. The first order correction $R_t^{(1)}$ encodes the effects of adiabatic pumping, and it will be discussed in Sec. 4.1. Higher order corrections $R_t^{(k>1)}$ can in general be neglected for the charge and the spin current ($R \in \{I_r, J_r\}$), as long as $\Omega \ll \Gamma$. This is however not true for the heat current [33], where contributions to second order in the driving frequency $Q_{r,t}^{(2)}$ account for heating effects due to the ac-driving, see Sec. 5.2.

3 Thermoelectric devices and heat currents In a thermoelectric device, an electric current can be generated as a result of an applied temperature difference ΔT . The underlying physical mechanism is perhaps easiest to understand in a ballistic device, where electrons can be transported between a hot and a cold metallic contact through a central region without losing energy, see Figs. 1 (a)-(c).

The larger smearing of the Fermi surface on the hot side results in a net current of high-energy electrons tunneling from the hot to the cold electrode, as well as a net current of low-energy electrons tunneling in the opposite direction. Therefore, if the conductance is energy independent [Fig. 1(a)], the total electric current is zero and only a heat current flows from the hot to the cold electrode. If, on the other hand, either high- or low-energy electrons are more easily transported through the central region [Fig. 1(b)], the electron currents no longer cancel each other and an electric current can flow as a result of the temperature difference, in addition to the heat current. This is the thermoelectric effect. Thus, a thermoelectric material must have different transport properties for electrons above and below the Fermi energy.

In an open circuit, the thermoelectric current will lead to charge accumulation in the electrodes and thereby a thermoelectric voltage, V , which will eventually be large enough to stop the net electric current, see Fig. 1(c). The proportionality constant, $S = -V/\Delta T$, is called the Seebeck coefficient or thermopower. The sign of the voltage depends on the direction of the thermally generated current and therefore on whether the electron or the hole conductance is largest.

3.1 Thermoelectric efficiency In order to perform useful electric work, the setup of Fig. 1 has to be modified to include an external electric circuit making use of the extracted power, which can simply be considered as a resistor, see Fig. 1(d). The efficiency η of a heat to electric power converter is given by the generated output electric power, $P = IV$, divided by the input heat power which has to be supplied to the hot electrode to keep it hot. If we neglect other heat losses, the needed input heat is equal to the heat current Q flowing from the hot to the cold electrode, and

$$\eta = \frac{IV}{Q}. \quad (4)$$

Since no heat engine operating between a hot and a cold heat bath can be more efficient than the ideal Carnot process, η is limited from above by $\eta_C = 1 - T_c/T_h$.

Commonly one considers only the linear regime, where $I = GV + G_T \Delta T$, where G is the electrical conductance and G_T the thermal conductance. The Seebeck coefficient is then $S = G_T/G$ and the heat current $Q = (\kappa_{el} + \kappa_{ph})\Delta T$, where κ_{el} and κ_{ph} are the electron and phonon contributions to the thermal conductance, respectively. A large η is related to a large thermoelectric figure of merit, ZT , with $T = (T_c + T_h)/2$, given by

$$ZT = \frac{GS^2T}{\kappa_{el} + \kappa_{ph}}. \quad (5)$$

In the linear response regime, the relation between ZT and η is [34]

$$\eta = \frac{\Delta T}{T_h} \frac{\sqrt{1 + ZT} - 1}{\sqrt{1 + ZT} + T_c/T_h}. \quad (6)$$

Today's best thermoelectrics are heavily doped narrow bandgap semiconductor materials with $ZT \approx 1$. Inserting $ZT = 1$ in Eq. (6) and assuming $T_h \approx T_c$, one finds $\eta \approx 0.17\eta_C$. Finding bulk materials with high ZT has proven to be more difficult than initially anticipated. One reason is that the ratio of the electronic thermal conductance and the electric conductance in bulk materials follows the Wiedemann-Franz law [35]

$$\frac{\kappa_{el}}{GT} = \frac{\pi^2 k_B^2}{3e^2}, \quad (7)$$

and increasing G is therefore accompanied by an increase in κ_{el} . Efforts to maximize the efficiency have instead focused on reducing κ_{ph} . The challenge is to achieve this without affecting G too much, which can be done by introducing effective phonon-scattering centers in the form of heavy-ion species with large vibrational amplitudes [36]. Recently, nanoscale engineering has been used to achieve this goal, e.g., using superlattice structures with an acoustic mismatch between the different layers, resulting in interfaces which scatter phonons more efficiently than electrons, which has resulted in impressive figures of merit ($ZT \approx 2.4$ in Ref. [37]). Superlattice structures require precise nanoscale engineering and are thus not suitable for large-scale production. Fortunately, it seems like the same positive effects can be achieved in non-periodic structures, such as nanocomposite materials consisting of a host material filled with nanoparticles [38,39], or by introducing roughness into Si nanowires [40].

Strictly speaking, Eq. (7) holds only for free electrons, but it is approximately valid in most bulk systems. Fortunately, several recent studies, see e.g., Refs. [41, 42,43], have shown that the Wiedemann-Franz law completely breaks down in nanoscale systems. The reason for this breakdown is either electron-electron interaction, or quantum confinement leading to effectively one- or two-dimensional structures. It is therefore useful to for the moment forget about the phonons ($\kappa_{ph} \rightarrow 0$) and ask the question: Which (electronic) material properties would actually maximize ZT as defined in Eq. (5)? And how large would this ZT be? This problem was studied and solved by Mahan and Soho [44]. They showed that the ideal material is characterized by the conductivity as a function of energy being proportional to the δ -function, where the peak should be localized $2.4k_B T$ above or below the Fermi level (giving an electron-type or a hole-type thermoelectric device). In this case, ZT goes to infinity and Carnot efficiency can be achieved (meaning reversible thermoelectric operation [45,46]). In practice of course $\kappa_{ph} > 0$ and ZT remains finite. Remembering that the origin of the thermoelectric effect is an energy asymmetry in the conductivity

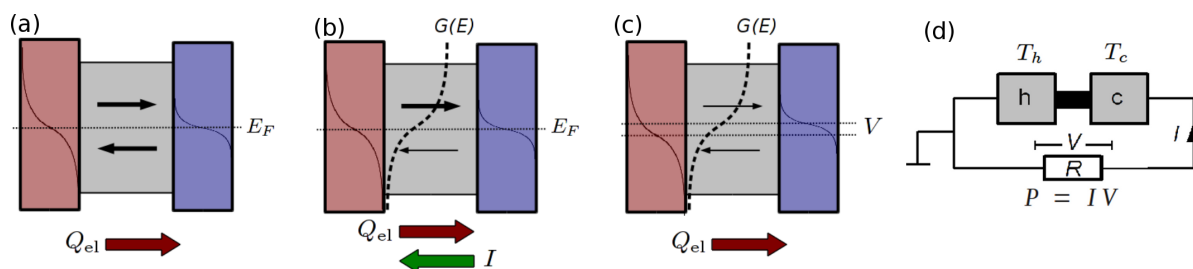


Figure 1 (a)–(c) Explanation of the thermoelectric effect. Red and blue rectangles indicate the conduction bands of the metallic hot and cold electrodes, respectively. The curved line represents the thermal smearing of the Fermi surface around the Fermi energy, E_F . (a) If the transport properties of the central region are the same for electrons above and below E_F , the temperature difference only results in an (electronic) heat current Q_{el} , but no net electric current. (b) If, on the other hand, the conductance $G(E)$ of the central region is larger (or smaller) for $E > E_F$, also a net (thermo)electric current I results from the temperature difference. (c) If the thermoelectric current is allowed to flow for some time in an open circuit, a (thermoelectric) voltage V builds up, which eventually cancels the electric current. (d) Sketch of thermoelectric circuit converting heat power, Q , supplied to the hot electrode, into electric power, P , in an electrically driven device (represented by a resistor, R).

[Fig. 1(b)], it is rather easy to understand the merits of a δ function, as it allows perfect energy filtering of the electrons passing through the material.

Mahan and Soho suggested using rare-earth compounds with very sharp electronic f -levels to achieve a δ -like conductivity, but correct alignment of these levels with respect to the Fermi energy is problematic, as is the phonon contribution to the heat current. A more modern way of introducing a strong energy asymmetry in the conductivity is to take advantage of nanostructuring to reduce the effective dimensionality of the system, since the density of states in low-dimensional systems is less smooth. Initial experiments focused on two-dimensional quantum wells, see e.g., Ref. [47], where the density of states is constant, with steps whenever a new 2D band becomes accessible. Also one-dimensional systems, such as nanowires [48,40] and carbon nanotubes [49,50], have been investigated, where the density of states has sharp peaks corresponding to the bottom of the 1D bands. In quantum dots, which are effectively zero-dimensional, the density of states has peaks corresponding to the discrete orbitals, and the conductance therefore resembles the δ -function shape. Several theoretical and experimental works have investigated the Seebeck effect in quantum dot devices, see e.g., Refs. [51,52,53,54]. However, quantum dots made in inorganic materials have level spacings of a few meV at the most, and the density of states therefore looks rather smooth at room temperature, which limits the usefulness for most applications. We will therefore now turn to molecular devices, since a molecule weakly coupled to electrodes behaves as a quantum dot, but with a level spacing which can be much larger than $k_B T$ also at room temperature.

First it should be mentioned, however, that achieving a high ZT is not all that matters for thermoelectric materials. Even with $ZT \rightarrow \infty$, Carnot efficiency can only

be reached in the limit of infinitely slow, reversible operation, where the device produces zero output power. It is therefore also interesting to look at intrinsically nonequilibrium quantities such as efficiency at maximum output power. Nonetheless, studies have indicated [20] that also in such cases a δ -like conductivity is desirable. One problem with a δ -like conductivity is that the actual output power is rather small. For example, if a zero-dimensional system is strongly coupled to electrodes to allow for a large current flow, and thereby large output power, the orbital states are broadened into Lorentzians, rather than δ functions, resulting in a decreased efficiency. Therefore, it was the conclusion of Ref. [55] that one-dimensional systems might be preferable when a high output power is desired.

3.2 Molecular thermoelectric devices The Seebeck effect was recently measured in single-molecule junctions, using an STM as sketched in Fig. 2(a), see Refs. [56, 57,58]. A gold substrate is covered with the molecules to

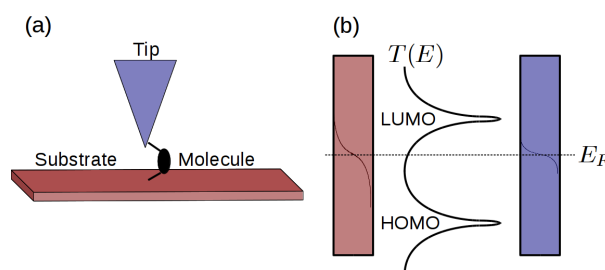


Figure 2 (a) Sketch of STM setup used to create single-molecule thermoelectric junctions. (b) Energy diagram of hot (red) and cold (blue) electrode, cf., Fig. 1. Between the electrodes the transmission function of the molecule, $T(E)$, is sketched, which shows peaks at the positions of the HOMO and LUMO.

be measured, which is then heated by passing a current through it (Joule heating), while the STM tip is kept at the ambient temperature. Conductance measurements are used to verify that a molecule is contacted. The tip–substrate voltage bias and current amplifier are then replaced by a voltage amplifier, which measures the induced thermoelectric voltage as the tip is slowly retracted from the substrate. When coupled to the tip and substrate contacts, the HOMO and LUMO of the molecules studied in Refs. [56,57,58] are far away from the electrode Fermi levels, transport is dominated by elastic (energy-conserving) tunneling and can be described by the Landauer–Büttiker formalism [59, 60,41]. The conductance of the molecular junction is then proportional to the transmission function at the Fermi energy, $G \propto T(E_F)$. Often, $T(E)$ is roughly proportional to the molecular density of states and has peaks at the positions of the HOMO and LUMO, see Fig. 2(b). As discussed above, the thermoelectric effect relies on electrons above and below the Fermi level having different conductances and in the zero-temperature limit it can be shown that

$$S \propto \frac{1}{T(E_F)} \frac{dT(E_F)}{dE}. \quad (8)$$

Therefore, the sign of the Seebeck coefficient gives an indication of whether the HOMO or LUMO lies closest to the Fermi level.

The Seebeck coefficients found in Refs. [56,57,58] were rather modest ($|S| < 10 \mu\text{V/K}$). Much higher values can be expected if either the HOMO or the LUMO lies closer to the Fermi level. Furthermore, a more narrow width of the transmission peaks increases the derivative of the transmission function in Eq. (8) and thereby the Seebeck coefficient, provided that the HOMO or LUMO position is adjusted appropriately. The width of the transmission peaks is set by the strength of the tunnel couplings to the electrodes and therefore a weak coupling is desirable to approach the δ -like conductivity of Mahan and Soho [44]. That a single-molecule junction can indeed, in theory, operate at ideal efficiency was the conclusion of Ref. [19], and Ref. [20] showed that such a device has a high efficiency even away from equilibrium. If it proves too difficult to move the HOMO or LUMO close enough to the Fermi level, or if small enough tunnel couplings cannot be achieved, an alternative is to use molecules with sharp features in the transmission function, for example Fano resonances [61], charge-Kondo resonances [62], “transmission supernodes” [63], or interference-related features [64,65], which also result in a strong energy-dependence of the conductance.

Naturally, a single molecule does not provide enough output power for an actual application as a power converter. Instead, a self-assembled molecular monolayer could be used. However, due to e.g., re-arrangement of molecular or surface charges or interactions between static molecular dipole moments [66,67,68], or inter-molecular tunnel-

ing [69,70,71,72], the transport properties of a molecular monolayer may be rather different compared with single-molecule devices. In addition, a recent theoretical study [73] showed that Coulomb interactions between charge carriers transported through neighboring molecules within a monolayer may significantly broaden the transport resonances. This might have a negative effect on the thermoelectric efficiency.

3.3 Electron–phonon coupling and phononic heat currents Having seen that the electronic properties of molecules hold promise for efficient thermoelectric power conversion, we now turn to important contributions to the losses in such devices, namely electron–phonon coupling and coupling between quantized molecular vibrations and substrate phonon modes in the electrodes.

Electron–phonon coupling is the coupling between the charge on the molecule and its vibrational motion. Due to the electron–phonon coupling, electrons tunneling through the molecule can excite it vibrationally [9,74,75,76]. In a simple picture, such inelastic processes destroy the δ -like character of the transmission function, since electrons can tunnel through the molecule at energies other than the conducting HOMO or LUMO, by either giving off excess energy into the molecular vibrations, or by absorbing vibrational energy from them. In a thermoelectric device, the relevant modes are those with a vibrational energy $\hbar\omega \sim k_B T$. Modes with much larger energies cannot be excited and those with much smaller energies do not contribute as much to heat losses. Thus, as will be substantiated below based on a simple model, in a good thermoelectric molecule all vibrational modes with $\hbar\omega \sim k_B T$ should have a small electron–phonon coupling [77].

In addition, the molecular vibrational modes couple to substrate phonon modes in the electrodes [74]. Essentially, the chemical bond between the molecular anchoring groups and the electrodes acts as a spring, which can transfer vibrational energy from the phonon modes in the hot electrode, into the molecular vibrations, and finally out again into the cold electrode phonons. The resulting phononic heat current has been analyzed in several theoretical works [78,79,80]. A strategy to minimize such losses is to choose molecules which form strong chemical bonds to the electrodes (meaning a stiff spring), such that all molecular vibrations with a significant amplitude at this bond have frequencies above the highest acoustical phonons in the electrodes. A strong chemical bond could be combined with a weak tunnel coupling, as needed to obtain sharp electronic resonances, e.g., by connecting the bonding atoms to the rest of the molecule through saturated carbon atoms, as in a methylene spacer [81]. However, a molecule in a transport junction has additional low-energy center-of-mass vibrational modes [82], which are likely below the Debye frequency of the electrodes.

3.3.1 A simple model of a molecule coupled to phonons To better understand the concepts discussed above, we now focus on a simple molecular model [77,83],

which still captures the relevant aspects of electronic and vibrational degrees of freedom. We model the molecule as a single spin-degenerate orbital level with energy ϵ and onsite Coulomb interaction U and include a single harmonic molecular vibrational mode with frequency ω . Furthermore, there is a linear electron–vibration coupling λ_{ph} between the electron occupation of the orbital and the vibrational coordinate. The transport characteristics of this so-called Anderson-Holstein model, when the molecular orbital is tunnel coupled to voltage biased source and drain electrodes, has been analyzed in many works, see e.g., [84, 85, 86, 87, 88, 89]. Here we consider instead a thermoelectric junction operated as a heat to electric power converter, where a hot electrode with temperature $T_h = T + \Delta T$ is grounded (chemical potential $\mu_h = 0$) and a (negative) voltage $-V$ is applied to the cold electrode ($\mu_c = V > 0$) with temperature $T_c = T$. Note that in an actual device which also makes use of the converted power, the voltage is not applied, but rather controlled by the temperature bias and the resistance of the external circuit, see Fig. 1(d). In addition to the electronic tunnel coupling, we include a coupling between the coordinate of the localized molecular vibration and a continuum of vibrational modes in the two electrodes. Electron tunneling between the molecule and electrode $r = h, c$ is associated with a rate Γ_r and the corresponding rate at which vibrational excitations “leaks” out from the molecule and into the electrode phonon modes is denoted by γ_r . As discussed above, the maximum efficiency of energy conversion is expected in the limit of weak electron tunneling and, of course, weak coupling between molecular vibrations and electrode phonons, meaning that $T \gg \Gamma_r, \gamma_r$.

In the weak coupling regime, the type of master equation introduced in Sec. 2 can be used to calculate the molecular density matrix describing both the electronic and vibrational state. The interplay between electron and phonon transport is nontrivial, as these processes interact via the vibrational distribution on the molecule (which is not necessarily thermalized). The electric and the electronic and phononic heat currents can be found as described in Sec. 2, and the efficiency is evaluated from Eq. (4), $\eta = P/Q_h$, where $P = IV$ with $I = -I_h = I_c$. Note that the relevant heat current is Q_h since the loss is given by the heat which must be supplied to keep this electrode hot. The distinction is important since there is no conservation of the stationary heat current. Instead, the first law of thermodynamics guarantees that $P = Q_h + Q_c$, so in fact, to obtain η , one could completely avoid calculating the electric current and instead calculate only Q_h and Q_c .

3.3.2 Optimal bias voltage and level position We start by studying the efficiency and output power at fixed thermal bias, here chosen to be $\Delta T = T$, as function of V and ϵ . The efficiency of a single level quantum dot (spinless electrons and no vibrational mode) was studied in Ref. [20], showing that Carnot efficiency is reached in the equilibrium limit of vanishing current. For vanishing

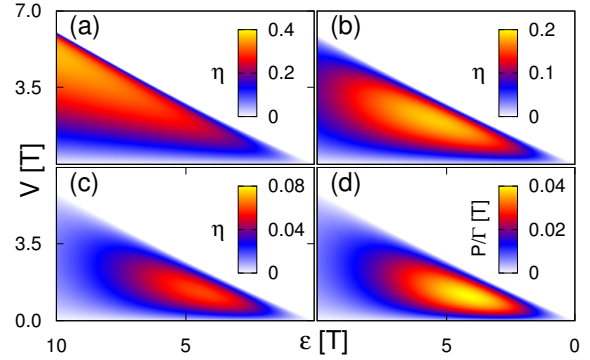


Figure 3 (a)–(c) η at $\Delta T = T$, as function of V and ϵ for increasing coupling to substrate phonons, $\gamma = 0$ (a), $\gamma = \Gamma/10$ (b), $\gamma = \Gamma$ (c). In all plots $\lambda_{\text{ph}} = 1$, $\omega = T$, $U = 10T$ and the couplings are symmetric, $\gamma_h = \gamma_c = \gamma$, $\Gamma_h = \Gamma_c = \Gamma$. (d) P as function of V and ϵ for the parameters used in (b) (the power depends only weakly on γ).

couplings to the phonon mode, $\gamma_r \rightarrow 0$ and $\lambda_{\text{ph}} \rightarrow 0$, this result remains valid in the non-interacting limit, $U = 0$, as well as for very strong interactions, $U \gg T, \Delta T$, while the efficiency is slightly reduced in the intermediate regime.

With finite λ_{ph} , but keeping $\gamma_r = 0$, the efficiency is decreased and never reaches the Carnot value, see Fig. 3(a). In fact, η vanishes close to the zero electric current line (boundary of the white area), the reason being that, in contrast to the single-level case, the heat current does not vanish completely when the charge current does. Inside the white area the current has been reversed by a too large voltage bias and flows from high- to low-biased electrode and therefore does not accomplish any useful electric work (note that this regime cannot be reached in the thermoelectric circuit of Fig. 1(d)). The maximal efficiency is reached when the level is far above the Fermi edges of both leads, where electron transport involves very few thermally excited states in the heated electrode and electron-induced vibrational excitations are exponentially suppressed, minimizing electronic heat loss. However, in this regime the current is highly suppressed, leading to a small output power, see Fig. 3(d). In addition, even a small coupling to the substrate phonons, $\gamma = \Gamma/10$ in Fig. 3(b), drastically decreases the efficiency in this low-current regime, while having a smaller effect in the regime where the current is larger (ϵ is smaller). Thus, even a weak coupling to substrate phonon modes, $\gamma \ll \Gamma$, drastically changes the ideal operating conditions for maximum η by introducing a heat loss which depends only weakly on ϵ and V . When the coupling to the substrate phonons becomes comparable to the tunnel coupling, $\gamma \approx \Gamma$ in Fig. 3(c), the efficiency is significantly decreased also in the high current regime.

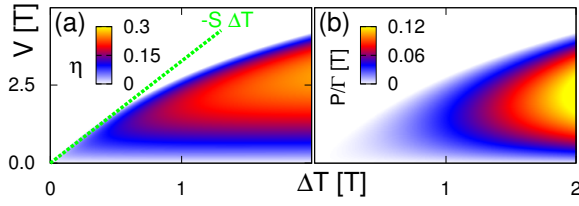


Figure 4 (a) η and (b) P as a function of V and ΔT , with $\epsilon = 5T$ and other parameters as in Fig. 3(b).

3.3.3 Temperature dependence and molecular heating Next we fix the level position to a value with both large power and efficiency, $\epsilon = 5T$, and vary instead V and ΔT . The resulting efficiency and output power is shown in Figs. 4(a) and (b) for the same parameters as in Fig. 3(b). As above, a too large voltage bias compared to the temperature bias reverses the current and no useful electric work is accomplished (white areas). The non-linear thermopower can be defined through $V = -S(\Delta T)\Delta T$ at $I = 0$, i.e., V is the finite voltage needed to compensate the temperature bias and give zero electric current. As expected, both efficiency and power are increased by an increased temperature bias.

Comparing Fig. 4(a) and (b), we see that for a given temperature bias, maximum efficiency and maximum output power is achieved at almost the same voltage bias. The reason is seen from the relation $P = \eta (Q_h^{(e)} + Q_h^{(p)})$, where $Q_h^{(e)}$ ($Q_h^{(p)}$) is the electron (phonon) contribution to the heat current. Since $Q_h^{(p)}$ only has a weak (indirect) dependence on the voltage bias, η and P can be simultaneously maximized by adjusting the bias when the phonon heat loss dominates ($\gamma \gg T$). As Fig. 4 shows, this holds approximately also when $\gamma \sim T$.

Ref. [77] investigated also the effects of $\lambda_{ph} > 1$, which further reduces both η and P , and $\lambda_{ph} < 1$, which increases η . Furthermore, both low- and high-energy vibrational modes ($\omega \ll T$ or $\omega \gg T$), have a much smaller effect on η . A low frequency mode can essentially be seen as a broadening of the electronic resonance of width $\sim \omega \lambda_{ph}^2$. Almost all decrease in efficiency in this case comes from the coupling to substrate phonon modes. A high-frequency mode, on the other hand, cannot be excited and therefore does not contribute at all to electron or heat transport.

4 Time-dependent driving and adiabatic pumping Charge or heat currents in an electric conductor are typically generated by imposing a voltage or temperature gradient between the electrodes of a device, as in the case of Sec.3. However, in a mesoscopic conductor, a dc-current can flow even without external gradients if some parameters of the system are periodically modulated in time [90]. When the modulation is slow compared to the characteristic time scales of the system, the transport mechanism is

called *adiabatic pumping*. In this case, the pumped charge depends only on the geometry of the pumping cycle in parameter space, i.e. it is of geometric nature [91,92]. The interest in adiabatic pumping has various motivations. For one, in appropriate modulation setups [93,94], the charge pumped per period is quantized in units of the electron charge. Adiabatic charge pumps are therefore promising candidates for a very precise current standard for metrology [26]. Furthermore, the controlled emission of single charges [25] is of interest for quantum information and electronic analogs of quantum optical effects [95]. In the opposite case where the transferred charge is not necessarily quantized, the pumping mechanism can be dominated by quantum effects [96]. This yields the possibility of revealing internal properties of the device which are not visible from standard transport spectroscopy through stationary setups. We will discuss examples for this *adiabatic transport spectroscopy* in the following sections.

In the last years, adiabatic pumping in solid-state devices has been widely studied both experimentally [97, 98, 27, 23, 99] and theoretically. As long as interactions can be treated on a self-consistent mean-field level [100], adiabatic pumping is well described by Brouwer's theory [101], which is based on a generalization of the scattering matrix approach for time-dependent phenomena [102]. This formalism has been applied to study several aspects of pumping in non-interacting systems, such as dissipation and noise [92, 21], and the possibility of spin-pumping [103, 104]. Further works dealt with different setups, including normal metal-superconductor hybrid structures [105, 106, 107], pumping by surface acoustic waves [108, 109], and graphene-based quantum pumps [110]. Heat currents have been considered as well in non-interacting electronic quantum-pumps, both in the limits of adiabatic [21] and non-adiabatic driving [111, 112, 113].

For systems dominated by a strong Coulomb interaction, the mean-field approach breaks down and new formulations are necessary to describe pumping. Several studies addressed interaction effects in specific setups and regimes. Pumping in interacting quantum wires has been discussed in Refs. [114, 115]. Pumping through open quantum dots was addressed in Ref. [116, 117] by employing bosonization techniques, while the Keldysh Green's function approach has been applied to investigate pumping in interacting quantum dots [118, 119], including the Kondo regime [120, 121, 122]. A diagrammatic real-time approach [29] was used to investigate several aspects of adiabatic pumping through interacting quantum-dot systems [30, 123, 124, 28, 125, 126] weakly coupled to the leads, and served as the basis for non-equilibrium renormalization group studies that treat the tunneling non-perturbatively [127].

Interestingly, adiabatic pumping effects, i.e. the occurrence of a finite flux in a preferred direction in response to a slow periodic or random zero-mean perturbation, are rel-

evant not only in solid-state mesoscopic devices, but also for ion-channels in cell membranes [128], enzymatic reactions [129] and, stochastic kinetics in general [130].

4.1 Geometric properties of adiabatic pumping

In terms of the master equation approach outlined in Sec. 2, adiabatic pumping is described by the contribution to the current to first order in the modulation frequency, $R_t^{(1)}$ ($R \in \{I_r, Q_r, J_r\}$). To emphasize its geometric aspects it is useful to introduce auxiliary vector fields in parameter space [91]. The key observation is that $R_t^{(1)}$ is directly related to the time derivative of the instantaneous occupation probabilities,

$$R_t^{(1)} = \text{Tr} \left\{ \mathcal{W}_t^R \tilde{\mathcal{W}}_t^{-1} \frac{d}{dt} P_t^{(0)} \right\} \equiv \varphi^R \frac{d}{dt} P_t^{(0)}, \quad (9)$$

where $\tilde{\mathcal{W}}_t^{-1}$ is a pseudo-inverse of the evolution Kernel [131]. In the second identity we introduced the vector-valued response coefficients φ^R , which describes for $R = I_r, Q_r, J_r$, the rate at which charge, heat and spin respectively, is transferred to lead r due to a change in the occupation probabilities. The average current pumped per period $\mathcal{T} = 2\pi/\Omega$, can then be written as a line-integral over a closed contour $\partial\Sigma$ in the space of the driving parameters [131, 132]

$$\bar{R}^{(1)} \equiv \mathcal{T}^{-1} \int_0^{\mathcal{T}} dt R_t^{(1)} = \mathcal{T}^{-1} \oint_{\partial\Sigma} d\mathbf{u} \cdot \mathcal{A}_R(\mathbf{u}), \quad (10)$$

with $\mathcal{A}_R = \sum_{\xi} \varphi_{\xi}^R(\mathbf{u}) \nabla P_{\xi}^{(0)}(\mathbf{u})$. The bar indicates that the average over one driving period has been taken. Here $\mathbf{u} = \sum_i u_i \mathbf{e}_i$ is the “position” vector in parameter space and $\nabla = \sum_i \mathbf{e}_i \partial_{u_i}$. The vector field \mathcal{A}_R can be interpreted as a pseudovector potential defined in the space of the driving parameters [131], and its components are directly related to the concept of emissivity [102, 119]. From Eq. (10) it follows directly that at least two independent driving parameters are required to have a non vanishing pumped current, $\bar{R}^{(1)} \neq 0$. In the case of two-parameters pumping, $\mathbf{u} = \{u_1, u_2\}$, using Stoke’s theorem, Eq. (10) can be written as the surface integral

$$\bar{R}^{(1)} = \mathcal{T}^{-1} \iint_{\Sigma} d\mathbf{S} \cdot \mathcal{B}_R(\mathbf{u}), \quad (11)$$

where $\mathcal{B}_R(\mathbf{u}) = \nabla \times \mathcal{A}_R(\mathbf{u})$ and $d\mathbf{S}$ is the directed surface element in parameter space. The average current $\bar{R}^{(1)}$ can then be seen as the flux of the pseudo-magnetic field \mathcal{B}_R . The advantage of this representation is that \mathcal{B}_R anticipates the conditions for finite pumping without referring to the specific details of the modulation [131].

The geometric interpretation holds however only to first order in the driving frequency and cannot be generalized to higher-order contributions, which depend sensitively on how the pumping orbit is traversed.

4.2 Adiabatic transport spectroscopy

In this section we will show how the geometric interpretation of adiabatic pumping can be used for the analysis of adiabatic transport spectroscopy. As an example we study a single-level quantum dot in a non-equilibrium regime induced by the modulation of the dot’s level position and the applied bias around a *finite value*. This situation has been addressed both in non-interacting systems [113, 133] within the context of the scattering matrix theory and, more recently, in a strongly interacting quantum dot weakly coupled to leads [28, 131]. We will focus on this last example and show that pumping is interaction-induced and can be used as a spectroscopic tool to access information on spin degeneracy and junction asymmetry in the quantum dot, complementing standard dc-spectroscopy (“stability diagrams”). Based on Sec. 4.1, we describe the interplay between interaction and non-equilibrium effects in terms of the pseudo-magnetic fields associated to the charge and spin currents. To this end, we consider the transport setup shown in Fig. 5(a). The quantum dot is described by the Hamiltonian $H_D(t) = \sum_{\sigma} (\epsilon(t) - \sigma\Delta/2) n_{\sigma} + U n_{\uparrow} n_{\downarrow}$, where Δ is the Zeeman splitting due to an applied external magnetic field and U is the onsite Coulomb energy. The level energy of the dot $\epsilon(t)$ is driven by a time-dependent gate voltage while the electro-chemical potentials in the reservoirs are controlled by the bias, i.e. $\mu_r(t) = \pm V(t)/2$ for $r = \{L, R\}$. These two voltages are slowly driven at frequency Ω in a circular orbit around a working point $(\bar{\epsilon}, \bar{V})$.

Following Sec. 2, the charge and spin currents $R \in \{I_r, J_r\}$ are calculated in lowest order in the coupling to the leads, and we will focus on the adiabatic correction (linear order in the modulation frequency) to the instantaneous solution. After a full cycle of the modulation, the net amount of charge/spin transferred to the r -lead is given by the instantaneous current flowing in response to the finite, time-dependent bias and the additional pumped charge/spin, $\mathcal{N}_R = \mathcal{T} \bar{R}^{(1)}$, generated by the delayed response. Experimentally, this adiabatic contribution can be extracted from the total current by using a lock-in technique. According to Sec. 4.1, it is possible to represent the average current, and hence \mathcal{N}_R , in terms of a pseudo-magnetic field which in this case reads as

$$\mathcal{B}_R(\mathbf{u}) = \nabla \varphi_n^R \times \nabla \langle n \rangle + \nabla \varphi_s^R \times \nabla \langle S_z \rangle, \quad (12)$$

with the driving parameters $\mathbf{u} = (\epsilon, V)$. Instead of occupation probabilities, Eq. (9), we here use the instantaneous dot’s average charge $\langle n \rangle_t$ and spin $\langle S_z \rangle_t$, respectively. The response coefficients $\varphi_{n,t}^R$ and $\varphi_{s,t}^R$ determine the amount of charge/spin leaving the r -lead when either the average charge or spin in the dot is changed in response to the driving.

In the non-interacting limit ($U = 0$), the response coefficients turn out to be independent of the driving parameters and hence they yield a zero pseudo-magnetic field such that the pumped charge and spin completely vanish. Adia-

batic pumping in the discussed regime is hence *interaction-induced*.

The finite pseudo-magnetic field generated by a large Coulomb charging energy ($U \gg T$) and zero magnetic field is shown in Fig. 5(b). A finite pumped charge occurs in peaks located around the meeting point of two dot level resonance lines (dashed lines in the figure); for the remaining regions B_{I_L} (and therefore the pumped charge) vanishes for the following reasons: (i) When the driving is far away from any resonance line, the occupation in the dot remains constant, and its time-derivative is hence zero. (ii) When the full driving trajectory only crosses a single resonance line, the response coefficient and the occupation number depend on the same effective parameter and hence their gradients are parallel.

The low-bias peaks (labeled by A and C), displayed in the “stability diagram for the pumped charge” in Fig. 5(b) are dominant, while the high-bias peaks (B and D) only emerge when a non-zero asymmetry $\lambda = (\Gamma_L - \Gamma_R)/\Gamma$ between left and right contacts is present. Moreover, the adiabatic pumping can here be used to directly identify the nature of the coupling asymmetry: the peaks A and B in Figs. 5(b), are related to each other by

$$\mathcal{B}_{I_L}^{(B)}(\epsilon, V) = \lambda \mathcal{B}_{I_L}^{(A)}(V/2, 2\epsilon). \quad (13)$$

Since $|\lambda| < 1$, the magnitude of the peak B is always smaller than the one of peak A and its *sign* is determined by the sign of the coupling asymmetry λ . For any two modulation curves centered around these points, a change of variables allows to write $\mathcal{N}_{I_L}^{(B)} = \lambda \mathcal{N}_{I_L}^{(A)}$, such that the mere presence of a pumped charge in the high-bias regime indicates an asymmetric coupling to the leads. Interestingly, this simple relation can be used for a direct quantitative estimation of the coupling asymmetry by dividing the independently measured values of pumped charges at the points B and A.

Note that in contrast to metrological applications of adiabatic pumping, the transferred charge is never quantized here. When the area enclosed by the modulation in parameter space includes a full peak, the pumped charge reaches however a plateau whose maximum value, corresponding to $\lambda = 0$, is $1/6$ in units of the electronic charge.

In the presence of a finite external magnetic field, Fig. 5(c), the resonances of Fig. 5(b) are split into further well-separated peaks. Interestingly, regardless of the value of λ , there is no peak at the zero-bias crossing points (black arrows). In this regime of the driving, the vector potentials for the charge and spin currents are irrotational, such that integration over a closed trajectory yields zero pumping. The reason for this is that a finite pumped charge requires not only a modulation encircling the meeting point of two resonance lines but also a change in the spin degeneracy of the ground state [28]. This requirement becomes evident for the crossing at $V = \Delta$, where the spin degeneracy is effectively recovered through the applied bias. Charge

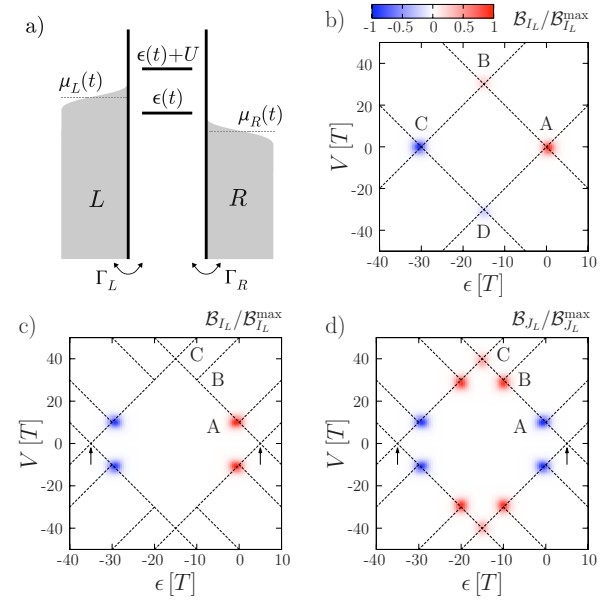


Figure 5 (a) Scheme of the transport device. (b) Stability diagram for the pumped charge: gate and bias map of the normalized pseudo-magnetic field for $\Delta = 0$ and $\lambda = 0.25$. Bottom panels: Normalized pseudo-magnetic fields for $\Delta = 10T$ associated to the pumped charge (c) and spin (d) for $\lambda = 0$. The chosen Coulomb interaction is $U = 30T$.

pumping is hence also an indicator of the spin degeneracy occurring in the level spectrum of a quantum dot.

4.3 Spin pumping In addition to charge pumping, the possibility to pump spin is an interesting option due to its significant robustness against environment decoherence. As fundamental elements in the realization of spin-based electronics, spin pumps could operate in a wide range of setups including ‘turnstile spin pumps’, i.e., quantum dots in presence of an external magnetic field where the spin current flows in response to a periodic modulation of the confining potentials [27, 103], or combinations of driving parameters like the coupling to the leads and the amplitude of the magnetic field [134]. Other interesting examples exploit the spin polarization in the reservoirs, like heterostructures consisting of normal metal and precessing ferromagnetic leads acting as a spin battery [135, 136], or quantum systems where the spin-orbit coupling is at the core of the phenomenon [104, 137]. In a double quantum dot coupled to normal metal and ferromagnetic contacts, pure spin pumping is obtained when modulating the level positions of the coupled dots [125].

Returning now to the setup of Fig. 5(a), an external magnetic field ($\Delta \gg T$) generates a spin current $J_{r,t}^{(1)}$ that flows through the dot in response to the time-dependent modulation. The above adiabatic spectroscopy of the resonance peaks for the pumped charge can also be extended to the spin degree of freedom, where one could test how

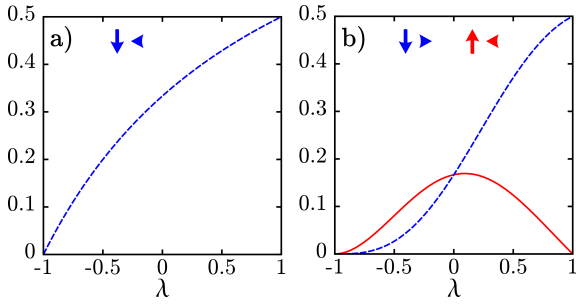


Figure 6 Absolute value for the spin-resolved pumped charge $\mathcal{N}_{I_L^\sigma} = (\mathcal{N}_{I_L} + 2\sigma\mathcal{N}_{J_L})/2$ for peaks A and B in Figs. 5(c) and (d). Directions for spin-up (solid red) and spin-down (dashed blue) pumped charge are denoted by arrows.

the pumped spin relates to the pumped charge at different biases. To this end, we consider an external magnetic field that induces a non-zero adiabatic spin current flowing through the dot.

In Fig. 5(d) we show stability diagrams for the pumped spin in the presence of a finite magnetic field, $\Delta \neq 0$. The difference between charge and spin fields is particularly pronounced for a symmetric junction ($\lambda = 0$), where *pure* spin pumping occurs in the high-bias regime: the pumped charge peaks B and D at high bias vanish exactly while those related to the pumped spin remain finite.

In Fig. 6 we show the spin-resolved pumped charge associated to the peaks of the pseudo-magnetic fields in Figs. 5(c) and (d). Its sign, independent of λ , fixes the direction of the overall current after one cycle of the driving, as indicated by the arrows in the figure. In panel (a), the pumped charge at peak A is fully polarized: transport of spin down from the right to the left lead causes the net flow of spin. Panel (b) shows the pumped charge at peak B. Strikingly, the pumped charge for the two spin orientations always flow in opposite directions. In the symmetric case $\lambda = 0$, their magnitudes are exactly the same, such that the total transported charge cancels out while the pumped spin remains finite. The same qualitative behavior is found also for the currents around the peak C.

Finally, this analysis can be extended to the remaining peaks in Figs. 5(b)-(d) by using the symmetries of the pseudo-magnetic fields around the particle-hole symmetry point $(\bar{\epsilon}, \bar{V}) = (-U/2, 0)$. Specifically, we find an antisymmetric shape for the pseudo-magnetic field associated to the pumped charge, i.e. $\mathcal{B}_{I_L}(-u) = -\mathcal{B}_{I_L}(u)$ whereas the one for the pumped spin is symmetric, i.e. $\mathcal{B}_{J_L}(-u) = \mathcal{B}_{J_L}(u)$.

5 Pumping heat with a driven double quantum dot In Sec. 3 we considered the performance of a molecular quantum dot as thermoelectric engine in the stationary state. The study of quantum-dot devices as nanoscale

engines can be extended to the case of time-dependently driven systems, where both the specific properties of the device and the external driving can now be exploited to perform useful work (e.g. by moving an electron from a lower to a higher chemical potential) or to cool a reservoir. In particular, the time-dependent modulation of a quantum-dot setup allows to realize mesoscopic analogs of cyclic heat engines that are sequentially coupled and decoupled to hot and cold reservoirs [138].

Here, we focus on the case of a double-dot pump (see Fig. 7a) which, differently from the single-dot setup of Sec. 4.2, permits pumping one electron per cycle even in the presence of a finite bias [97,99]. Moreover, it allows for the implementation of an efficient effective decoupling scheme from the reservoirs. The double dot is described by the Hamiltonian $H_D = \sum_r \epsilon_r n_r + U n_L n_R + \frac{U'}{2} \sum_r n_r (n_r - 1) - \frac{t_c}{2} \sum_\sigma (d_{L\sigma}^\dagger d_{R\sigma} + \text{h.c.})$, where $n_r = \sum_\sigma d_{r\sigma}^\dagger d_{r\sigma}$ is the occupation number operator of dot $r = L, R$ and ϵ_r the corresponding single-particle energy, which can be modulated in time by external gates $\epsilon_r = \epsilon_r(t)$. Interactions between electrons in the same or in different dots are accounted for by U' and U , while t_c represents the inter-dot tunneling amplitude. In the following, we will assume the onsite interaction U' to be the largest energy scale in the system – so that each dot can be at most singly occupied – and consider the case of strong inter-dot coupling $t_c \gg \Gamma$. Finally, we assume that the system is symmetrically tunnel coupled to two non-interacting electronic reservoirs, which are in equilibrium at the temperatures $T_L = T + \Delta T$ and $T_R = T$ and chemical potentials $\mu_L = -\mu_R = V/2$.

The standard “honeycomb” stability diagram of the double dot is shown in Fig. 7(b), and identifies regions of different equilibrium occupation numbers for the two dots, as a function of the energies ϵ_L and ϵ_R . The regions where three charge states are degenerate are named *triple points*. The pump is operated by applying a sinusoidal voltage to the local gates of the two dots with a $\pi/2$ phase shift between them, which forces the state of the system to follow a circular orbit in parameter space, see e.g. Fig. 7(c).

5.1 Quantized charge and heat pumping We consider first the case of pure *adiabatic pumping*, ($\Delta T = 0$, $V = 0$ and $\Omega \rightarrow 0$), where the only relevant contributions to the currents are those to first order in the driving frequency Ω , i.e., $R^{(1)}(t)$. As discussed in Sec. 4.1, the average current $\bar{R}^{(1)}$ has a geometric interpretation and it can be expressed as the flux of the pseudo magnetic field \mathcal{B}_R through the area in parameter space enclosed by the pumping cycle. The pseudo magnetic fields associated with charge and heat pumping through the double dot are shown in Figs. 7(c)-(d). They exhibit features localized at the triple points. If the pumping orbit is large enough to fully encircle one of these features, the charge and heat pumped per period become independent of the details of the pumping cycle and the resulting dc-currents show plateaux with height $\bar{I}_L^{(1)} = \pm \frac{\Omega}{2\pi}$ and $\bar{Q}_L^{(1)} = \pm \frac{\Omega}{2\pi} T \ln 2$, see Fig. 8.

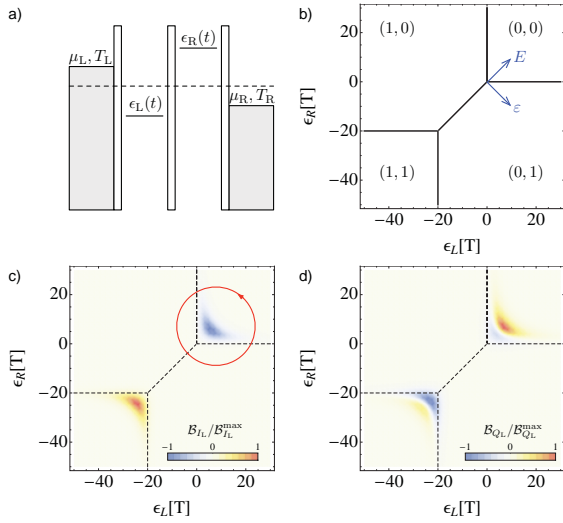


Figure 7 (a) Sketch of the potential landscape of a double-dot setup. (b) Stability diagram of the double dot for the case $V = 0$, and $\Delta T = 0$: black lines indicate the borders of the stability regions for negligible inter-dot coupling. The system of coordinates formed by the detuning $\varepsilon = \varepsilon_L - \varepsilon_R$ and the mean energy $E = (\varepsilon_L + \varepsilon_R)/2$ is also shown. (c) Color scale plot of the pseudo magnetic field associated with charge pumping B_L (normalized to its maximum value) and sketch of a possible pumping trajectory in parameter space. (d) Color scale plot of the pseudo magnetic field associated with heat pumping B_Q . In panels (b)-(d): $U = 20T$, $t_c = 10T$, $\Gamma \ll T$.

While the appearance of plateaux in the charge current is directly related to the quantization of charge, plateaux in the heat current reflect the degeneracies occurring in the double dot. This can be understood by noticing that along an orbit that fully encloses a triple point, whenever one of the two dots comes in resonance with its neighboring lead, the other one is strongly off-resonant, so that particles are exchanged only with one lead at the time. In this case, the average heat current flowing from each lead $\bar{Q}_r^{(1)}$ is directly related to the difference in entropy in the double dot before and after an electron has tunneled through the r barrier, $\bar{Q}_r^{(1)} = T \Delta S_r^{(0)}$, where, $S^{(0)} = -\sum_{\xi} P_{\xi}^{(0)} \ln P_{\xi}^{(0)}$ is the Shannon entropy of the double dot and the subscript r indicates that the entropy difference is between two charge configurations that differ only by one electron in dot r [33]. In this case where the double dot states are spin-degenerate, we have $\Delta S_r^{(0)} = \pm \ln 2$.

5.2 Double-dot pump as a Carnot engine. An important feature of the double-dot pump is the possibility of achieving quantized pumping even in the presence of a finite bias voltage V or temperature gradient ΔT . This requires minimizing the contributions of the instantaneous currents $\bar{R}^{(0)}$, which play the role of leakage currents since they flow in the direction set by the gradient, irrespec-

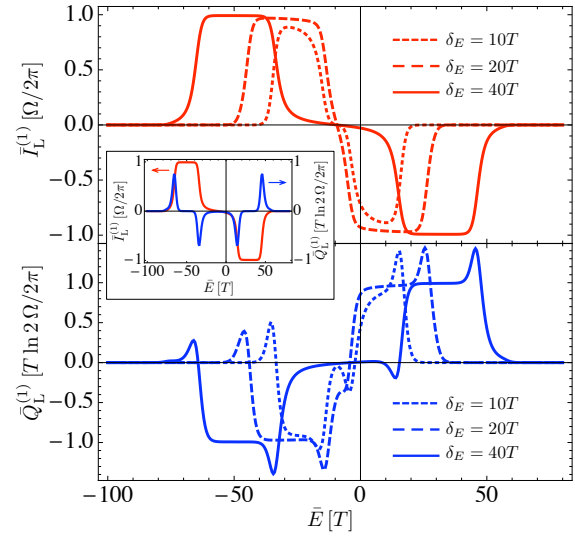


Figure 8 Upper panel: Average pumped charge-current plotted as a function of the mean energy \bar{E} , for three different pumping orbits. The pumping cycle is defined by: $E(t) = \bar{E} + \delta_E \sin(\Omega t)$ and $\varepsilon(t) = 2\delta_E \cos(\Omega t)$, where E is the mean energy and δ_E the driving amplitude (see Fig. 7(b)). Lower panel: same as above, but for the pumped heat-current. Inset: Average pumped charge and heat current for the case of a fully spin-polarized system. In all panels: $\Delta T = 0$, $V = 0$ and $U = 20T$, $t_c = 10T$, $\Gamma \ll T$.

tively of the orientation of the pumping cycle. This can be achieved by choosing a pumping cycle that fully encircles a single triple point. The triple point regions are broadened by V and ΔT . However, as long as they are well separated from each other, it remains possible to pump one electron per cycle through the double dot and the heat currents in each lead exhibit well defined plateaux of height $\frac{\Omega}{2\pi} T_r \ln 2$, where T_r is the local temperature of the lead [33]. In other words, even if the system is globally brought out of equilibrium, the heat exchanged solely with one lead obeys Clausius relation $\bar{Q}_r^{(1)} = T_r \Delta S_r^{(0)} \frac{\Omega}{2\pi}$. This is because along an orbit that fully encircles a triple point, the double dot is effectively coupled only to one lead at the time. In the limit of slow driving $\Omega \rightarrow 0$, the system has time to equilibrate with the lead it is coupled to, so that processes that change the total occupation of the double dot represent isothermal transitions between equilibrium states. A pumping cycle that fully encloses a triple point can then be regarded as a nanoscale analog of the Carnot cycle, in which two isothermal transitions are connected by two thermodynamically adiabatic transitions, i.e., occurring at constant entropy. The latter transitions accompany the crossing of the two dots' levels.

When the double dot is operated between two leads with different temperatures and same chemical potential, it acts either as a refrigerator or as heat engine, depending on the direction of the cycle. In the first case, a power

\mathcal{P}_{ac} has to be provided by the external ac-fields to extract heat from the cold reservoir. The efficiency of a refrigerator is characterized by its coefficient of performance $COP = \bar{Q}_{cold}/\mathcal{P}_{ac}$, where \bar{Q}_{cold} is the average heat-flow out of the cold reservoir. *Vice versa*, if heat is extracted from the hot reservoir and released in the cold one, work is performed on the external fields and the double dot functions as a heat engine. Its performance is characterized by the efficiency coefficient $\eta = (-\mathcal{P}_{ac})/\bar{Q}_{hot}$, with $(-\mathcal{P}_{ac})$ the work per unit time *done by the system* on the ac-fields and \bar{Q}_{hot} the heat absorbed from the hot lead. It is straightforward to show that in the ideal limit in which leakage currents can be completely neglected: we have $COP = T_{cold}/(T_{hot} - T_{cold})$ for the case of the cooling-cycle and $\eta = (T_{hot} - T_{cold})/T_{hot}$ for the heat engine, meaning that the double-dot pump can be operated with Carnot efficiency for $\Omega \rightarrow 0$ [33].

The efficiency of a realistic double-dot engine, is however limited both by the leakage currents $\bar{R}^{(0)}$ and by dissipative effects associated to a finite driving frequency. These are captured by the contribution to the currents to second order in the driving frequency, $\bar{R}^{(2)}$, which for the heat current is of the order of $\bar{Q}_r^{(2)} \sim \delta_E \Omega^2 / \Gamma$. This is the heat dissipated in each cycle due to the injection of hot electrons or holes into the leads. As discussed in Ref. [33], it can pose severe limitations to the efficiency of a double-dot based engine, especially in the regime of small ΔT . These limitations are less strict if one considers the operation of a double-dot pump as nanoscale “battery charger” performing work against a dc-source. In this case efficiencies up to 70% of the ideal value can be achieved, see Ref. [33].

Acknowledgements We acknowledge H. Schoeller for initial collaboration within the SPP-1243, K. Flensburg for collaborations, and financial support from the DFG under Contract No. SPP-1243, the Excellence Initiative of the German Federal State Government, and from the Ministry of Innovation NRW. ML additionally acknowledges financial support from the Swedish Research Council (VR) and nmC@LU.

References

- [1] A. T. Johnson, L. P. Kouwenhoven, W. de Jong, N. C. van der Vaart, C. J. P. M. Harmans, and C. T. Foxon, *Phys. Rev. Lett.* **69**, 1592 (1992).
- [2] R. Hanson, L. P. Kouwenhoven, J. R. Petta, S. Tarucha, and L. M. Vandersypen, *Rev. Mod. Phys.* **79**, 1217 (2007).
- [3] S. D. Franceschi, J. A. van Dam, E. P. A. M. Bakkers, L. F. Feiner, L. Gurevich, and L. P. Kouwenhoven, *Appl. Phys. Lett.* **83**, 344 (2003).
- [4] T. S. Jespersen, M. Aagesen, C. Sørensen, P. E. Lindelof, and J. Nygård, *Phys. Rev. B* **74**, 233304 (2006).
- [5] H. A. Nilsson, P. Caroff, C. Thelander, M. Larsson, J. B. Wagner, L. E. Wernersson, L. Samuelson, and H. Q. Xu, *Nano Lett.* **9**, 3151 (2009).
- [6] M. Bockrath, D. H. Cobden, P. L. McEuen, N. G. Chopra, A. Zettl, A. Thess, and R. E. Smalley, *Science* **275**, 1922 (1997).
- [7] S. J. Tans, M. H. Devoret, H. Dai, A. Thess, R. E. Smalley, L. J. Geerligs, and C. Dekker, *Nature* **386**, 474 (1997).
- [8] J. Güttinger, F. Molitor, C. Stampfer, S. Schnez, A. Jacobsen, S. Dröschner, T. Ihn, and K. Ensslin, *Rep. Prog. Phys.* **75**, 126502 (2012).
- [9] H. Park, J. Park, A. K. L. Lim, E. H. Anderson, A. P. Alivisatos, and P. L. McEuen, *Nature* **407**, 57 (2000).
- [10] S. Kubatkin, A. Danilov, M. Hjort, J. Cornil, J. Brédas, N. Stühr-Hansen, P. Hedegård, and T. Bjørnholm, *Nature* **425**, 698 (2003).
- [11] H. S. J. van der Zant, Y. V. Kervennic, M. Poot, K. O'Neill, Z. de Groot, J. M. Thijssen, H. B. Heersche, N. Stühr-Hansen, T. Bjørnholm, D. Vanmaekelbergh, C. A. van Walree, and L. W. Jenneskens, *Faraday Discuss.* **131**, 347 (2006).
- [12] L. P. Kouwenhoven, D. G. Austing, and S. Tarucha, *Rep. Prog. Phys.* **64**, 701 (2001).
- [13] D. V. Averin and K. K. Likharev, *J. Low Temp. Phys.* **62**, 345 (1986).
- [14] A. A. Clerk, M. H. Devoret, S. M. Girvin, F. Marquardt, and R. J. Schoelkopf, *Rev. Mod. Phys.* **82**, 1155 (2010).
- [15] F. Giazotto, T. T. Heikkilä, A. Luukanen, A. M. Savin, and J. P. Pekola, *Rev. Mod. Phys.* **78**, 217 (2006).
- [16] D. Loss and D. D. Vincenzo, *Phys. Rev. A* **57**, 120 (1998).
- [17] H. L. Edwards, Q. Niu, and A. L. de Lozanne, *Appl. Phys. Lett.* **63**, 1815 (1993).
- [18] J. R. Prance, C. G. Smith, J. P. Griffiths, S. J. Chorley, D. Anderson, G. A. C. Jones, I. Farrer, and D. A. Ritchie, *Phys. Rev. Lett.* **102**, 146602 (2009).
- [19] P. Murphy, S. Mukerjee, and J. Moore, *Phys. Rev. B* **78**, 161406(R) (2008).
- [20] M. Esposito, K. Lindenberg, and C. van den Broeck, *Eur. Phys. Lett.* **85**, 60010 (2009).
- [21] M. Moskalets and M. Büttiker, *Phys. Rev. B* **66**, 035306 (2002).
- [22] L. P. Kouwenhoven, A. T. Johnson, N. C. van der Vaart, C. J. P. M. Harmans, and C. T. Foxon, *Phys. Rev. Lett.* **67**, 1626–1629 (1991).
- [23] N. E. Fletcher, J. Ebbecke, T. J. B. M. Janssen, F. J. Ahlers, M. Pepper, H. E. Beere, and D. A. Ritchie, *Phys. Rev. B* **68**, 245310 (2003).
- [24] B. Kaestner, V. Kashcheyevs, S. Amakawa, M. D. Blumenthal, L. Li, T. J. B. M. Janssen, G. Hein, K. Pierz, T. Weimann, U. Siegner, and H. W. Schumacher, *Phys. Rev. B* **77**, 153301 (2008).
- [25] G. Fève, A. M. J. M. Berroir, T. Kontos, B. Plaças, D. C. Glatli, A. Cavanna, B. Etienne, and Y. Jin, *Science* **316**, 1169 (2007).
- [26] J. P. Pekola, O. P. Saira, V. F. Maisi, A. Kemppinen, M. Möttönen, Y. A. Pashkin, and D. V. Averin, *arXiv:1208.4030* (2012).
- [27] S. K. Watson, R. M. Potok, C. M. Marcus, and V. Umansky, *Phys. Rev. Lett.* **91**, 258301 (2003).
- [28] F. Reckermann, J. Splettstoesser, and M. R. Wegewijs, *Phys. Rev. Lett.* **104**, 226803 (2010).
- [29] J. Splettstoesser, M. Governale, J. König, and R. Fazio, *Phys. Rev. B* **74**, 085305 (2006).
- [30] F. Cavaliere, M. Governale, and J. König, *Phys. Rev. Lett.* **103**, 136801 (2009).

- [31] J. König, H. Schoeller, and G. Schön, *Phys. Rev. Lett.* **76**, 1715 (1996).
- [32] J. König, J. Schmid, H. Schoeller, and G. Schön, *Phys. Rev. B* **54**, 16820 (1996).
- [33] S. Jürgens, F. Haupt, M. Moskalets, and J. Splettstoesser, *arXiv:1303.5225* (2013).
- [34] K. H. Müller, *J. Chem. Phys.* **129**, 044708 (2008).
- [35] N. W. Ashcroft and N. D. Mermin, *Solid State Physics* (Henry Holt and Company, New York City, 1976).
- [36] H. Kim, M. Kaviani, J. C. Thomas, A. Van der Ven, C. Uher, and B. Huang, *Phys. Rev. Lett.* **105**, 265901 (2010).
- [37] R. Venkatasubramanian, E. Siivola, T. Colpitts, and B. O'Quinn, *Nature* **413**, 597 (2001).
- [38] R. Yang and G. Chen, *Phys. Rev. B* **69**, 195316 (2004).
- [39] M. S. Dresselhaus, G. Chen, M. Tang, R. Yang, H. Lee, D. Wang, Z. Ren, J. P. Fleurial, and P. Gogna, *Adv. Mater.* **19**, 1043 (2007).
- [40] A. I. Hochbaum, R. Chen, R. D. Delgado, W. Liang, E. C. Garnett, M. Najarian, A. Majumdar, and P. Yang, *Nature* **451**, 6381 (2008).
- [41] N. J. Appleyard, J. T. Nicholls, M. Pepper, W. R. Tribe, M. Y. Simmons, and D. A. Ritchie, *Phys. Rev. B* **62**, 16275(R) (2000).
- [42] D. Boese and R. Fazio, *Eur. Phys. Lett.* **56**, 576 (2001).
- [43] B. Kubala, J. König, and J. Pekola, *Phys. Rev. Lett.* **100**, 066801 (2008).
- [44] G. D. Mahan and J. O. Sofo, *Proc. Natl. Acad. Sci. U. S. A.* **93**, 7436 (1996).
- [45] T. E. Humphrey, R. Newbury, R. P. Taylor, and H. Linke, *Phys. Rev. Lett.* **89**, 116801 (2002).
- [46] T. E. Humphrey and H. Linke, *Phys. Rev. Lett.* **94**, 096601 (2005).
- [47] L. D. Hicks, T. C. Harman, X. Sun, and M. S. Dresselhaus, *Phys. Rev. B* **53**, 10493(R) (2010).
- [48] A. I. Boukai, Y. Bunimovich, J. Tahir-Kheli, J. K. Yu, W. A. Goddard III, and J. R. Heath, *Nature* **451**, 168 (2008).
- [49] J. P. Small, K. M. Perez, and P. Kim, *Phys. Rev. Lett.* **91**, 256801 (2003).
- [50] M. C. Llaguno, J. E. Fischer, A. T. Johnson, and J. Hone, *Nano Lett.* **4**, 45 (2004).
- [51] C. W. J. Beenakker and A. A. M. Staring, *Phys. Rev. B* **46**, 9667 (1992).
- [52] M. Turek and K. A. Matveev, *Phys. Rev. B* **65**, 115332 (2002).
- [53] R. Scheibner, E. G. Novik, T. Borzenko, M. König, D. Reuter, A. D. Wieck, H. Buhmann, and L. W. Molenkamp, *Phys. Rev. B* **75**, 041301 (2007).
- [54] S. F. Svensson, A. I. Persson, E. A. Hoffmann, N. Nakpathomkun, H. A. Nilsson, H. Q. Xu, L. Samuelson, and H. Linke, *New J. Phys.* **14**, 033041 (2012).
- [55] N. Nakpathomkun, H. Q. Xu, and H. Linke, *Phys. Rev. B* **82**, 235428 (2010).
- [56] P. Reddy, S. Y. Jang, R. A. Segalman, and A. Mujumdar, *Science* **315**, 1568 (2007).
- [57] K. Baheti, J. A. Malen, P. Doak, P. Reddy, S. Y. Jang, T. D. Tilley, A. Mujumdar, and R. A. Segalman, *Nano Lett.* **8**, 715 (2008).
- [58] J. A. Malen, P. Doak, P. Reddy, K. Baheti, T. D. T. R. A. Segalman, and A. Majumdar, *Nano Lett.* **9**, 1164 (2009).
- [59] R. Landauer, *IBM J. Res. Develop.* **1**, 223 (1957).
- [60] M. Büttiker, *Phys. Rev. Lett.* **57**, 1761 (1986).
- [61] C. M. Finch, V. M. García-Suárez, and C. J. Lambert, *Phys. Rev. B* **79**, 033405 (2009).
- [62] S. Andergassen, T. A. Costi, and V. Zlatić, *Phys. Rev. B* **84**, 241107 (2011).
- [63] J. P. Bergfield, M. A. Solis, and C. A. Stafford, *ACS Nano* **4**, 5314 (2010).
- [64] G. C. Solomon, D. Q. Andrews, T. Hansen, R. H. Goldsmith, M. R. Wasielewski, R. P. Van Duyne, and M. A. Ratner, *J. Chem. Phys.* **129**, 054701 (2008).
- [65] O. Karlström, H. Linke, G. Karlström, and A. Wacker, *Phys. Rev. B* **84**, 113415 (2011).
- [66] R. Naaman and Z. Vager, *MRS Bulletin* **35**, 429 (2010).
- [67] G. Heimel, F. Rissner, and E. Zojer, *Adv. Mater.* **22**, 2494 (2012).
- [68] D. A. Egger, F. Rissner, E. Zojer, and G. Heimel, *Adv. Mater.* **24**, 4403 (2012).
- [69] S. N. Yaliraki and M. A. Ratner, *J. Chem. Phys.* **109**, 5036 (1998).
- [70] M. Magoga and C. Joachim, *Phys. Rev. B* **59**, 16011 (1999).
- [71] M. G. Reuter, G. C. Solomon, T. Hansen, T. Seideman, and M. A. Ratner, *J. Phys. Chem. Lett.* **2**, 1667 (2011).
- [72] M. G. Reuter, T. Seideman, and M. A. Ratner, *Nano Lett.* **11**, 4693 (2011).
- [73] M. Leijnse, *Phys. Rev. B* **87**, 125417 (2013).
- [74] S. Braig and K. Flensberg, *Phys. Rev. B* **68**, 205324 (2003).
- [75] A. N. Pasupathy, J. Park, C. Chang, A. V. Soldatov, S. Lebedkin, R. C. Bialczak, J. E. Grose, L. A. K. Donev, J. P. Sethna, D. C. Ralph, and P. L. McEuen, *Nano Lett.* **5**, 203 (2005).
- [76] E. A. Osorio, K. O'Neill, N. Stühr-Hansen, O. F. Nielsen, T. Bjørnholm, and H. S. J. van der Zant, *Adv. Mater.* **19**, 281 (2007).
- [77] M. Leijnse, M. R. Wegewijs, and K. Flensberg, *Phys. Rev. B* **82**, 045412 (2010).
- [78] D. Segal and A. Nitzan, *J. Chem. Phys.* **117**, 3915 (2002).
- [79] D. Segal, *Phys. Rev. B* **73**, 205415 (2006).
- [80] M. Galperin, A. Nitzan, and M. A. Ratner, *Phys. Rev. B* **75**, 155312 (2007).
- [81] K. Moth-Poulsen and T. Bjørnholm, *Nature nanotechnology* **4**, 551 (2009).
- [82] J. S. Seldenthuis, H. S. J. van der Zant, M. A. Ratner, and J. M. Thijssen, *ACS Nano* **2**, 1445 (2008).
- [83] M. Galperin, A. Nitzan, and M. A. Ratner, *Molecular Physics* **106**, 397 (2008).
- [84] K. Flensberg, *Phys. Rev. B* **68**, 205323 (2003).
- [85] A. Mitra, I. Aleiner, and A. J. Millis, *Phys. Rev. B* **69**, 245302 (2004).
- [86] J. Koch and F. von Oppen, *Phys. Rev. Lett.* **94**, 206804 (2005).
- [87] J. Koch, F. von Oppen, and A. V. Andreev, *Phys. Rev. B* **74**, 205438 (2006).
- [88] F. Haupt, F. Cavaliere, R. Fazio, and M. Sassetti, *Phys. Rev. B* **74**, 205328 (2006).

- [89] M. Leijnse and M. R. Wegewijs, *Phys. Rev. B* **78**, 235424 (2008).
- [90] D. J. Thouless, *Phys. Rev. B* **27**, 6083 (1983).
- [91] J. E. Avron, A. Elgart, G. M. Graf, and L. Sadun, *Phys. Rev. B* **62**, R10618 (2000).
- [92] Y. Makhlin and A. D. Mirlin, *Phys. Rev. Lett.* **87**, 276803 (2001).
- [93] Q. Niu and D. J. Thouless, *J. Phys. A: Math. Gen.* **17**, 2453 (1984).
- [94] J. E. Avron, A. Elgart, G. M. Graf, and L. Sadun, *Phys. Rev. Lett.* **87**, 236601 (2001).
- [95] E. Bocquillon, V. Freulon, J. M. Berroir, P. Degiovanni, B. Plaças, A. Cavanna, Y. Jin, and G. Fève, *Science* **339**, 1054 (2013).
- [96] F. Zhou, B. Spivak, and B. Altshuler, *Phys. Rev. Lett.* **82**, 608 (1999).
- [97] H. Pothier, P. Lafarge, C. Urbina, D. Esteve, and M. H. Devoret, *Europhys. Lett.* **17**, 249 (1992).
- [98] M. Switkes, C. M. Marcus, K. Campman, and A. C. Gosard, *Science* **283**, 1905 (1999).
- [99] S. J. Chorley, J. Frake, C. G. Smith, G. A. C. Jones, and M. R. Buitelaar, *Appl. Phys. Lett.* **100**, 143104 (2012).
- [100] M. Büttiker, *J. Phys.: Condens. Matter* **5**, 9361 (1993).
- [101] P. W. Brouwer, *Phys. Rev. B* **58**, R10135 (1998).
- [102] M. Büttiker, H. Thomas, and A. Prêtre, *Z. Phys. B* **94**, 133–137 (1994).
- [103] E. R. Mucciolo, C. Chamon, and C. M. Marcus, *Phys. Rev. Lett.* **89**, 146802 (2002).
- [104] M. Governale, F. Taddei, and R. Fazio, *Phys. Rev. B* **68**, 155324 (2003).
- [105] J. Wang, Y. Wei, B. Wang, and H. Guo, *Appl. Phys. Lett.* **79**, 3977 (2001).
- [106] M. Blaauboer, *Phys. Rev. B* **65**, 235318 (2002).
- [107] F. Taddei, M. Governale, and R. Fazio, *Phys. Rev. B* **70**, 052510 (2004).
- [108] Y. Levinson, O. Entin-Wohlman, and P. Wölfle, *Phys. Rev. Lett.* **85**, 634 (2000).
- [109] O. Entin-Wohlman, Y. Levinson, and P. Wölfle, *Phys. Rev. B* **64**, 195308 (2001).
- [110] E. Prada, P. San-Jose, and H. Schomerus, *Phys. Rev. B* **80**, 245414 (2009).
- [111] L. Arrachea, M. Moskalets, and L. Martin-Moreno, *Phys. Rev. B* **75**, 245420 (2007).
- [112] M. Rey, M. Strass, S. Kohler, P. Hänggi, and F. Sols, *Phys. Rev. B* **76**, 085337 (2007).
- [113] M. Moskalets and M. Büttiker, *Phys. Rev. B* **69**, 205316 (2004).
- [114] R. Citro, N. Andrei, and Q. Niu, *Phys. Rev. B* **68**, 165312 (2003).
- [115] S. Das and S. Rao, *Phys. Rev. B* **71**, 165333 (2005).
- [116] I. L. Aleiner and A. V. Andreev, *Phys. Rev. Lett.* **81**, 1286 (1998).
- [117] P. W. Brouwer, A. Lamacraft, and K. Flensberg, *Phys. Rev. B* **72**, 075316 (2005).
- [118] J. Splettstoesser, M. Governale, J. König, and R. Fazio, *Phys. Rev. Lett.* **95**, 246803 (2005).
- [119] E. Sela and Y. Oreg, *Phys. Rev. Lett.* **96**, 166802 (2006).
- [120] T. Aono, *Phys. Rev. Lett.* **93**, 116601 (2004).
- [121] A. Schiller and A. Silva, *Phys. Rev. B* **77**, 045330 (2008).
- [122] L. Arrachea, A. L. Yeyati, and A. Martin-Rodero, *Phys. Rev. B* **77**, 165326 (2008).
- [123] J. Splettstoesser, M. Governale, and J. König, *Phys. Rev. B* **77**, 195320 (2008).
- [124] N. Winkler, M. Governale, and J. König, *Phys. Rev. B* **79**, 235309 (2009).
- [125] R. P. Riwar and J. Splettstoesser, *Phys. Rev. B* **82**, 205308 (2010).
- [126] R. P. Riwar, J. Splettstoesser, and J. König, *Phys. Rev. B* **87**, 195407 (2013).
- [127] O. Kashuba, H. Schoeller, and J. Splettstoesser, *Europhys. Lett.* **98**, 57003 (2012).
- [128] R. D. Astumian, *Phys. Rev. Lett.* **91**, 118102 (2003).
- [129] N. A. Sinitsyn and I. Nemenman, *Eur. Phys. Lett.* **77**, 58001 (2007).
- [130] N. A. Sinitsyn, *J. Phys. A: Math. Theor.* **42**, 193001 (2009).
- [131] H. L. Calvo, L. Classen, J. Splettstoesser, and M. R. Wegewijs, *Phys. Rev. B* **86**, 245308 (2012).
- [132] J. Ren, P. Hänggi, and B. Li, *Phys. Rev. Lett.* **104**, 170601 (2010).
- [133] O. Entin-Wohlman, A. Aharony, and Y. Levinson, *Phys. Rev. B* **65**, 195411 (2002).
- [134] M. Blaauboer and C. M. L. Fricot, *Phys. Rev. B* **71**, 041303 (2005).
- [135] A. Brataas, Y. Tserkovnyak, G. E. W. Bauer, and B. I. Halperin, *Phys. Rev. B* **66**, 060404 (2002).
- [136] N. Winkler, M. Governale, and J. König, *Phys. Rev. B* **87**, 155428 (2013).
- [137] S. Rojek, J. König, and A. Shnirman, *Phys. Rev. B* **87**, 075305 (2013).
- [138] M. Esposito, R. Kawai, K. Lindenberg, and C. Van den Broeck, *Phys. Rev. E* **81**, 041106 (2010).